Characterization of Multimode Fiber by Selective Mode Excitation

Joel Carpenter and Timothy D. Wilkinson

***Abstract*—Each mode of a 2 km 50 μm OM2 grade multimode fiber is precisely excited at multiple orientations using a binary phase spatial light modulator (SLM) to generate a detailed modal description of the fiber and minimize modal dispersion over 4.5 THz of optical bandwidth.**

***Index Terms*—Adaptive optics, optical fiber communication, optical fiber dispersion, spatial light modulators.**

I. Introduction

PRECISE modal excitation in optical fibers is of interest for improving the transmission capacity of few-mode and multimode fibers either by minimizing modal dispersion in a single-channel [1]–[4] or as part of a mode-division multiplexing (MDM) system [5]–[15] where independent channels of information are propagated on different modes, or groups of modes. It is also of relevance to the characterization of novel fibers [16].

The more precise methods [3]–[9] of modal excitation typically have been by way of systems similar to that outlined in Fig. 1. With the exception of [3] which used a mask containing both amplitude and phase information, the mask takes the form of the phase of the far-field of the desired modal pattern. As the modes are described by real-only functions, they have only two possible phase states and hence the masks are binary, containing regions of either 0 or π phase delay. Although the amplitude information of the far-field is discarded by such a method, it can still be used to generate a good approximation of the desired mode. This is true particularly in the context of few-mode fibers, where the fiber itself provides additional spatial filtering. A better approximation to the desired mode can be achieved by including some amplitude information in the plane of the phase mask by use of a circular aperture optimized for each individual mode [4] or similarly by optimizing the mode-field diameter (MFD) of the beam illuminating the mask. However this has the practical drawback of requiring a physical adjustment of the aperture and/or lens focal length for each desired mode. In any case, the mode fields generated by such methods are still only rough approximations and as the number of modes supported by the fiber increases, it becomes increasingly difficult to maintain selective excitation of individual modes. The ability of MDM to offer significant bandwidth improvements is contingent on its ability to use a great many modes. This requires masks capable of precise generation of the desired modal fields. Similarly in the context of fiber characterization, it is difficult to perform accurate measurements on highly-modal fibers without precise mode launch.

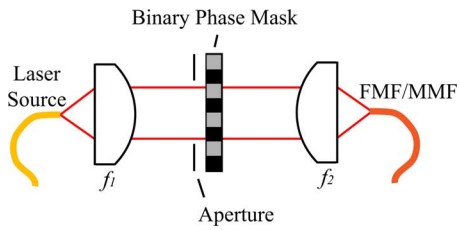

Fig. 1. Basic arrangement for modal excitation in few-mode (FMF) or multimode (MMF) fiber using a phase mask.

In this paper, highly selective binary phase masks are calculated using techniques from computational holography which generate modes of near perfect theoretical quality under the constraints of the system it is to operate in. That is, all modes can be excited at will with the same physical system, without the need to optimize focal lengths or aperture sizes.

The rotational dependence of modal performance has also been largely overlooked by previous work. Although the orientation of the mode is arbitrary and rotationally invariant for an ideal fiber, any actual fiber will have this symmetry broken by bends, twists and other imperfections in its geometry. This is similar to the way orthogonal polarizations, which ideally are completely degenerate, in practice propagate differently. Rotating the modal profiles is impractical using etched phase masks, which would need to be physically rotated, but is trivial when implementing the masks on a liquid-crystal based spatial light modulator (SLM).

The modal characteristics of the fiber are also investigated over wavelength, spanning the C-band, to verify that a single phase mask at a single shared orientation is capable of operating over a wide optical bandwidth for use in applications such as DWDM but also for measuring chromatic dispersion of individual modes and providing an estimate of the refractive index profile and peak dopant concentration.

II. Mode Generation

When selectively exciting modes in a fiber using a phase-only mask some variation of Fig. 1 is typically employed. Light from the laser source, usually a single-mode fiber is collimated through the first lens of focal length f_1. This beam may or may not pass through an aperture before transmitting through, or reflecting off, the phase mask which may be implemented as a

Manuscript received December 01, 2011; revised February 13, 2012; accepted February 13, 2012. Date of current version April 04, 2012.

The authors are with the Electrical Engineering Division, Department of Engineering, University of Cambridge, Cambridge, CB3 0FA, U.K. (e-mail: jac240@cam.ac.uk; tdw13@cam.ac.uk).

Color versions of one or more of the figures in this paper are available online at http://ieeexplore.ieee.org.

Digital Object Identifier 10.1109/JLT.2012.2189756

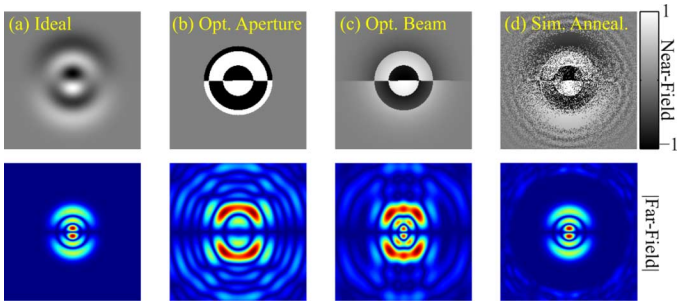

Fig. 2. Comparison of different mode excitation techniques. (a) Ideal launch with full amplitude and phase information. (b) Phase-only of the Fourier transform of the desired mode with an aperture of optimal diameter [4]. (c) Same phase mask as (b) but with optimized Gaussian beam waist diameter. (d) Mask calculated by simulated annealing.

fixed etching on glass [3], [7]–[9] or on a liquid-crystal based SLM [4]–[6]. The beam is then refocused into the output fiber through another lens with focal length f_2 which has typically been equal to f_1 [4], [6]. The mask itself has previously taken the form of the phase of the Fourier transform of the desired mode profile and as fiber modes are similar in both the near and far-fields, these profiles are nearly identical to the modes themselves. However encoding only the phase information in the plane of the phase mask (near-field) and discarding the amplitude content results in a far-field pattern which only approximates the desired mode. As mentioned in the introduction, some additional amplitude information can be reintroduced by the use of an aperture [4] or by optimizing the size of the beam waist illuminating the mask by adjusting the ratio between the focal lengths f_1 and f_2 of Fig. 1.

A qualitative example of these approaches can be seen in Fig. 2(b) and (c), respectively. When compared to the ideal case of Fig. 2(a) these methods result in undesirable side lobes and other artifacts which distort the quality of the mode. When working with a few-mode fiber [5]–[9] the fact that these profiles much more closely resemble the desired mode than any other supported mode of the fiber means the selectivity of the launch is still very high. The field may not have an ideal overlap with the desired mode, but it has virtually nonexistent overlap with any of what are few other modes of the fiber. Hence the power not in the desired mode simply becomes a coupling loss, rather than an excitation of an undesirable mode. However as more and more modes are supported there is less and less spatial filtering being performed by the fiber itself and it becomes increasingly likely that this remaining power will overlap with an undesired mode and degrade the selectivity of the launch. In particular it becomes increasingly difficult to distinguish between modes with similar symmetries, for example $\mathrm{LP}_{0,1}$ and $\mathrm{LP}_{0,2}$, or $\mathrm{LP}_{1,1}$ and $\mathrm{LP}_{1,2}$.

The technique employed in this paper uses a "simulated annealing" [17] based algorithm to create a binary phase mask which better approximates the desired field as can be seen in Fig. 2(d). The algorithm starts with an array of pixels in random states and optimizes by flipping random pixels one at a time, evaluating the corresponding change in the overlap of the far-field with the desired mode in a region slightly larger than the core of the fiber, and makes a decision on whether to accept or

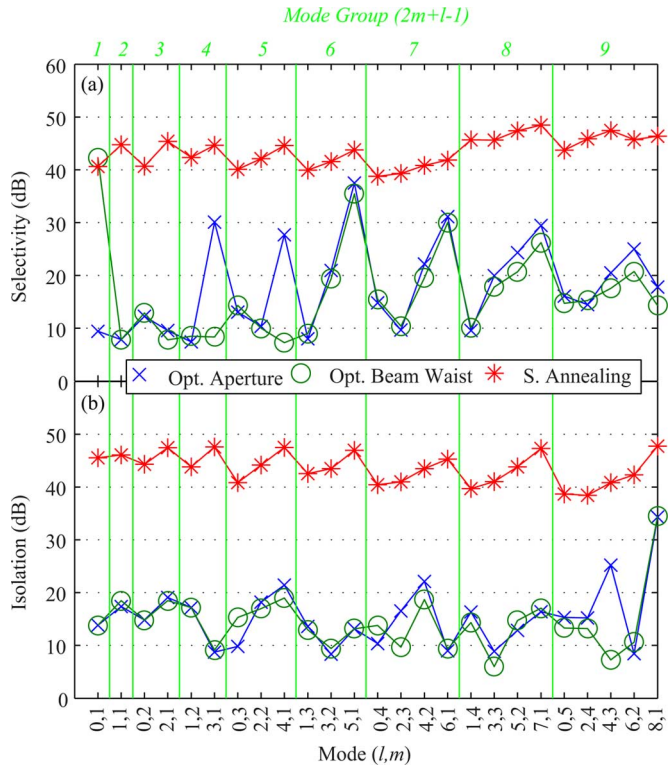

Fig. 3. Comparison of modal performance of masks generated using simulated annealing, and those of the simpler methods illustrated in Fig. 2.

reject the change based on the statistics of simulated annealing. To accelerate computation the algorithm is implemented on a graphics processing unit (GPU) which allows all the modes of the fiber to be calculated in parallel. In Fig. 2(d), it is apparent that in contrast with the methods of Fig. 2(b) and (c) the noise power has been distributed away from the core resulting in a highly selective launch. This method also works to optimize the phase mask under the constraints of a shared beam waist for all modes. Hence any mode can be excited with similar selectivity simply by reprogramming the SLM displaying the phase mask, without any mechanical change of the aperture or focal lengths. It also allows high selectivity to be maintained when using "off the shelf" optics where only discrete focal length options are available.

Fig. 3 is a quantitative comparison of the methods for a standard 50 μm core graded-index multimode fiber at 1550 nm. Degenerate modes are grouped together. For example power coupled into either of $\mathrm{LP}_{1,1a}$ and $\mathrm{LP}_{1,1b}$ corresponding to orthogonal orientations of the same mode, are both tallied under as a single value for $\mathrm{LP}_{1,1}$. Selectivity in this context refers to how much total power is coupled to undesired modes relative to the desired mode. Isolation is more relevant to MDM applications where each mode of the fiber is excited simultaneously with separate phase masks. Here isolation refers to the ratio of power coupled into the desired mode using the relevant phase mask, with the sum of the power coupled into that same mode due to all other phase masks, where the power of the mode excited by the relevant phase mask is held constant across all masks.

The aperture optimized results are for a plane-wave illuminating a phase mask with a circular aperture, the diameter of

which has been selected to optimize the total power in the far-field which is coupled into the desired mode. This corresponds with the example of Fig. 2(b). Similarly the beam waist optimized results illuminate the same phase masks as for the aperture optimized case but with a Gaussian beam selected in a similar fashion and without a circular aperture. This corresponds with the example of Fig. 2(c). The simulated annealing results use a fixed Gaussian beam with mode field diameter (MFD) of 77% the width of the phase mask for all modes. The calculation also includes the slight truncation of the beam by the finite extent of the phase mask. The optimized aperture and beam waist approaches can achieve decent results for some modes but worst-case selectivity and isolation is around 7 dB. If a fixed beam waist for all masks is employed of the same diameter as that used for the simulated annealing case, the selectivity drops to a worst case of less than 0 dB. That is, the mask is exciting more power in undesired modes than the desired mode. It is difficult for these simpler phase masks to maintain selectivity over a wide range of higher and lower order modes using a common illuminating beam size.

Clearly the simulated annealing approach yields superior results with both isolation and selectivity in excess of 38 dB for all modes and it does so without any requirement to tailor the optics of the system for each mode. It is also worth noting that the optimization process for the simulated annealing algorithm aimed to optimize the overlap with the desired mode in a given region near the core of the fiber, rather than directly optimizing the selectivity or isolation. Hence it could be possible to achieve higher theoretical quality using a more direct approach. However such high isolation and selectivity is already beyond what is likely in any real system particularly due to mode-coupling in the fiber, but also due to tolerances and imperfections in any actual implementation.

Examples of the actual far-field observed for some different calculated phase masks displayed on an SLM are shown in Fig. 4. In Fig. 4(c) it is possible to see the faint presence of the zeroth diffractive order of the SLM. This is a Fourier transformed version of the beam which illuminates the SLM and corresponds with light which has passed through the system without being influenced by the pattern displayed on the SLM. Imperfections in any actual system, such as dead space between the pixels, unwanted reflections or imperfect polarisers will give rise to some proportion of the light being undiffracted and travelling directly along the optical axis. This can be mitigated by use of better quality optics, particularly the SLM, or by offsetting the modal pattern from the optic axis. Offsetting the pattern would result in a slight drift in the position of the mode over wavelength and if the mask was constrained to only two phase levels an offset would also incur a 3-dB power penalty due to the conjugate symmetry property of the Fourier transform of a real-only function.

III. Experimental Investigation

A. Mode Excitation System

The system used to selectively excite the modes of the fiber is shown in Fig. 5. It starts with a C-band tunable laser which is modulated by a Mach–Zehnder modulator (MZM) driven by

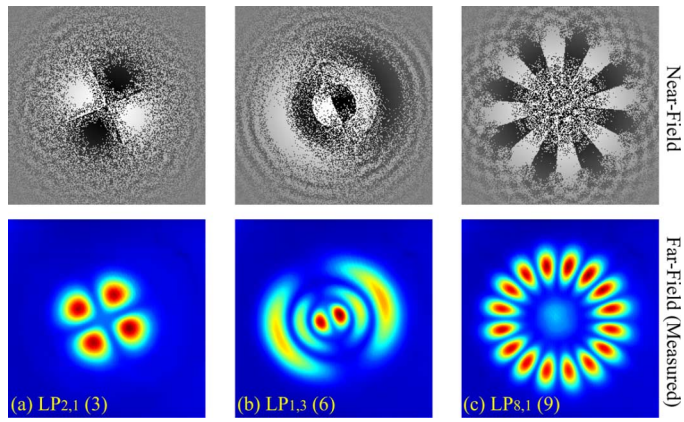

Fig. 4. Examples for three different modes $\mathrm{LP}_{l,m}$ (mode-group $2m + l - 1$). Theoretical near-field distribution (top) with experimentally observed far-field (bottom).

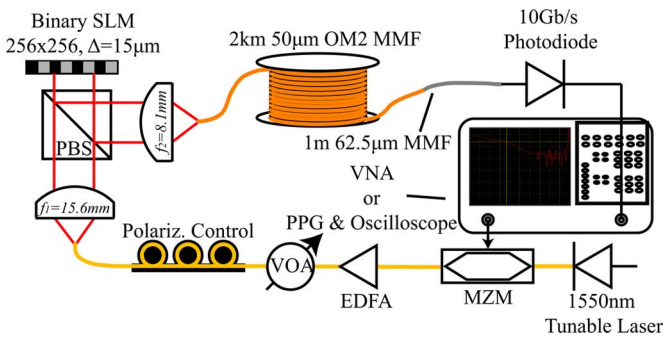

Fig. 5. Experimental setup used to modally characterize a multimode fiber.

either a pulse pattern generator (PPG) or vector network analyzer (VNA) depending on the experiment being conducted. The signal is then amplified by an erbium doped fiber amplified (EDFA) before passing through a variable optical attenuator (VOA). Next is a manual polarization controller which aligns the state of polarization leaving the fiber with that required to be transmitted through the polarizing beam splitter (PBS). The beam leaving the fiber is collimated through the first lens f_1 and passes through the PBS onto the SLM which is programmed with a phase mask corresponding to a particular mode at a particular orientation as detailed in the previous section. The ferroelectric liquid crystal based pixels of the SLM independently modulate the polarization of the incident beam between one of two states which upon reflection back through the PBS becomes a binary phase modulation. This beam is then Fourier transformed through the final lens f_2 which produces the desired mode at the core of the fiber under test. The fiber in this instance is a 2 km length of OM2 grade multimode fiber which has been measured to have an overfill launch (OFL) bandwidth of 940 MHz at 1548.5 nm (193.6 THz). At the receiving end, the fiber is coupled to a short length of 62.5 μm core multimode fiber connected to a custom made device based around a 10 Gb/s PIN photodetector (Finisar PIN-1310-10LR-SC) which is connected to the oscilloscope or VNA.

When conducting experiments using the VNA, the wavelength is swept across the C-band in 10 steps of 500 GHz for each phase mask for a total of 325 masks corresponding to

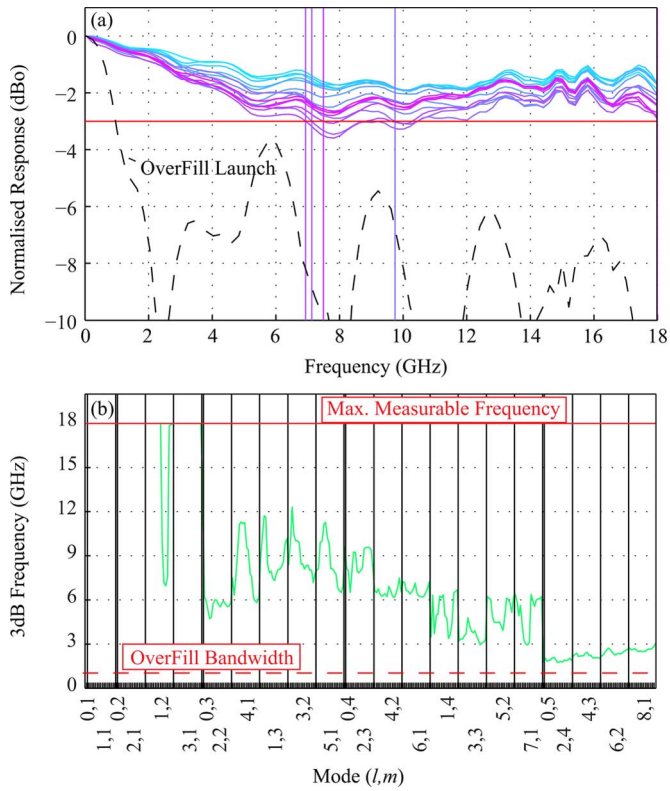

Fig. 6. Dependence of the 3-dB roll-off frequency on the orientation of the mode. (a) An example of this dependence for the $\mathrm{LP}_{1,2}$ mode. (b) 3-dB frequency for all 325 holograms representing all modes at various orientations.

25 modes spanning 9 mode-groups each at 16 different orientations. The EDFA is automatically adjusted by the control software to keep the power at the receiver constant regardless of the phase mask. The raw uncalibrated data is downloaded from the VNA and the response of the MZM, EDFA, and photodetector are all removed by a wavelength dependent calibration applied externally in software. Although the VNA is capable of measuring up to 20 GHz, due to the heavy frequency roll-off of the MZM and photodetector at these frequencies and the sensitivity of the VNA, it is only possible to calibrate the system reliably up to around 18 GHz.

B. Rotational Dependence on Modal Performance

In an ideal fiber the degenerate forms of a mode are completely identical in performance and the choice of orientation for a mode launch is completely arbitrary. In reality bends and twists in the fiber as well as manufacturing imperfections break this symmetry and different orientations of the same mode may not perform exactly the same. Take for example Fig. 6(a) where an $\mathrm{LP}_{1,2}$ mode at 1548.5 nm has been launched into the fiber at 16 different orientations. This rotational variation is also visible in Fig. 6(b) where the 3-dB roll-off frequency of that mode is shown to suddenly dip down to around 7 GHz for a few orientations. By rotating the mode to find a preferential axis of orientation it is possible to minimize modal coupling and achieve better performance in the context of telecommunications, or more accurately measure the modal properties when characterizing a fiber.

C. Modal Characterization of the Fiber

The refractive index of the core of a graded-index fiber is typically modeled as

$$n^2(r) = n_{\mathrm{core}}^2\left(1 - 2\Delta\left(\frac{r}{a}\right)^{\alpha}\right) \tag{1}$$

where r is the radial distance from the centre of the fiber, n_{core} is the peak refractive index, a is the total radius of the core, Δ is the profile height parameter $(n_{\mathrm{core}}^2 - n_{\mathrm{clad}}^2)/2n_{\mathrm{core}}^2$ and α is the profile parameter which is typically about 2 so as to minimize the difference in propagation delay between the different modes of the fiber. In the simplified case of a parabolic profile $(\alpha = 2)$ which extends to infinity without any constant refractive index cladding, the solutions of Maxwell's equations for the fiber can be solved analytically and modes can be organized into mode-groups $(2m + l - 1)$ which have degenerate propagation constants and group delays [18]. In reality, the existence of the cladding breaks this degeneracy; however modes within a mode-group still share almost identical propagation constants, leading to strong mode-coupling. The spread of group delays within a mode-group induced by the cladding is more significant for the higher order modes which have a larger proportion of their field propagating in the cladding.

By individually launching each mode at multiple orientations it is possible to measure the modal characteristics of the fiber. Fig. 7(a) and (b) illustrate the same measurements of the fiber response measured with a VNA in both the frequency and time-domain representations where the mode has been orientated so as to maximize the 3-dB rolloff frequency for that mode. The first 6 modes, corresponding with the first four mode-groups, have clearly defined propagation delays. Modes within these groups share almost identical delays which are distinct from the delays of all other modes. Moving towards higher-order groups there is a trend of increasingly poor performance which can be seen in the time-domain as more diffuse peaks with less consistent mode-group propagation delays, and as a faster rolloff in the frequency domain. The modes of group 9 arrive with a wide spread of delays, but delays which are distinct from the other groups. Even in the absence of modal coupling between different mode-groups this could be expected due to the skew in delays induced by the cladding as mentioned above and as visible in the green simulated constant α no-defect example of Fig. 8(b).

D. Modally Resolved Chromatic Dispersion

By sweeping the wavelength of the laser it is possible to measure the chromatic dispersion of the individual modes as shown in Fig. 8. In this case each mode has been launched at its optimal orientation for that wavelength. Although the chromatic dispersion of individual modes has been measured before [20]–[25], this is to the author's knowledge the first time more than 5 modes have been characterized.

Although the actual constituent glasses of the fiber under test are not known for certain, as a reference the measurements to follow are compared with theoretical calculations based around a fiber with a GeO_2 doped silica core inside a pure silica

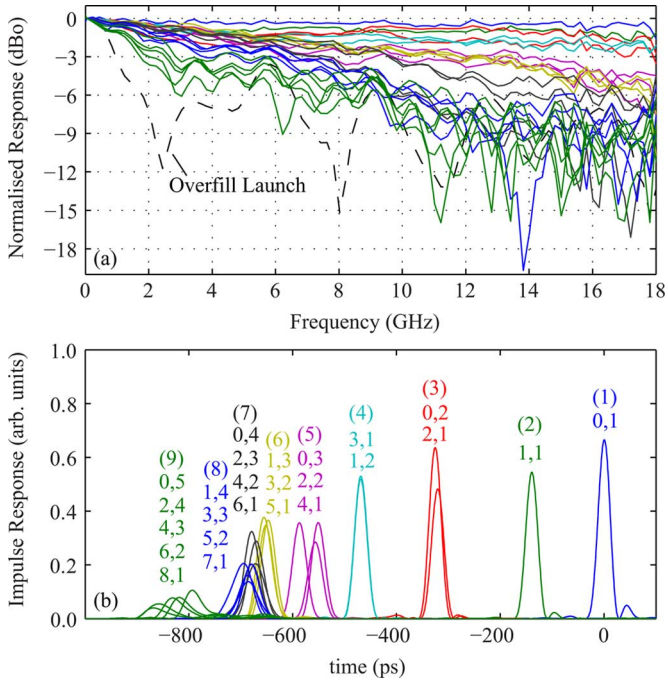

Fig. 7. (a) Normalized frequency response for all 25 modes at their optimal orientations at 1548.515 nm. (b) The Fourier transform of those same frequency responses representing the impulse response in the time-domain.

cladding. The fiber is assumed to have a doping profile which is similar in form to (1)

$$X(r) = X_{\text{core}}\left(1 - \left(\frac{r}{a}\right)^{\alpha}\right) \tag{2}$$

where X is the concentration (% mol) of GeO_2 as a function of radius, which drops from a peak of X_{core} at the centre of the core to 0% where the core meets the pure silica cladding.

The chromatic dispersion of the lowest order modes is almost entirely due to material dispersion and as a consequence, they are useful for providing an estimate of the peak dopant concentration in the core, in this case it is consistent with a concentration of approximately 13.5%. The relative propagation times of the other modes imply an α value which for the delays measured suggest $\alpha \approx 1.835$. GeO_2 doped silica is less dispersive than pure silica [18] and it can be seen from Fig. 8(c) that the chromatic dispersion of the higher order modes slowly increases as more of the mode propagates in the outer core and cladding with lower dopant concentration. As the mode order increases however the waveguide dispersion becomes increasingly negative [25], at first gradually, but dropping sharply as the modes near cutoff. In Fig. 8(c) this can be seen as the sudden drop in chromatic dispersion for the highest mode-group signifying that it is nearing cutoff.

The simulated results do not take into account mode coupling of any kind and the early arrival of the higher-order modes compared with that expected of a constant $\alpha = 1.835$ could simply be due to coupling between these mode-groups. This technique cannot distinguish between modes that arrive early or late due to coupling between mode-groups induced by bends and twists in the fiber and any deviation in mode delay which may occur

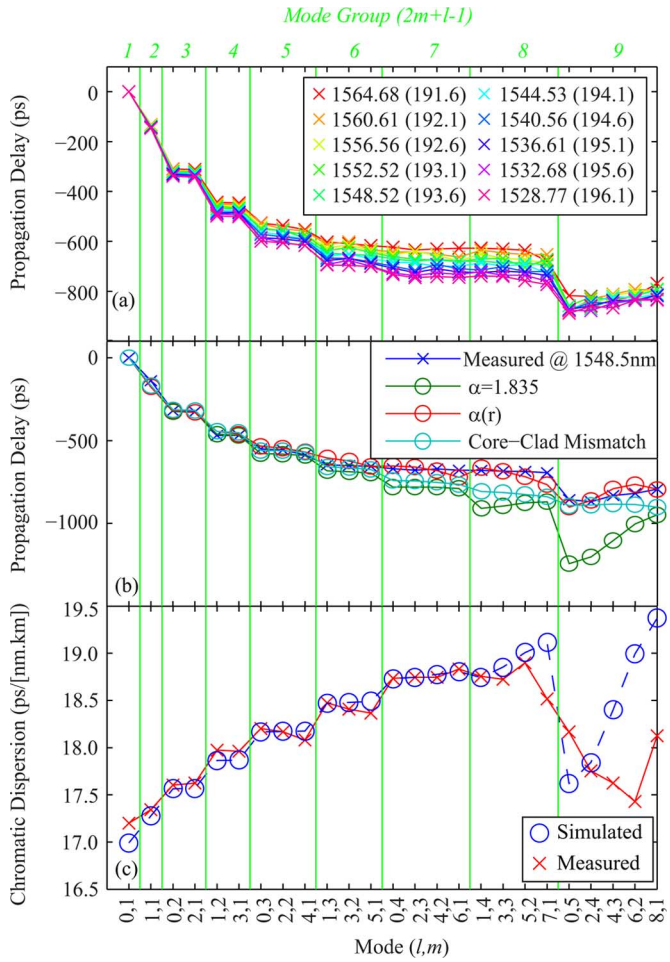

Fig. 8. Change in propagation delays for each mode over a 4.5 THz optical bandwidth. (a) In terms of total delay relative to the fundamental. (b) Measured delays at 1548.5 nm compared with some simulate refractive index profiles outlined in (3)–(6). (c) Normalized on a per km basis and compared with that expected of a 13.5% GeO_2 doped fiber with a constant $\alpha = 1.835$ profile parameter. Chromatic dispersion is derived from difference in delay measured at 1564.68 and 1528.77 nm in (a).

due to refractive index profile defects skewing the group delay and/or propagation constants of the modes. As the actual refractive index profile of the fiber is unknown, the simulated results of Fig. 8 are given as a reference to illustrate that the experimentally observed results are consistent with realistic profiles for this type of fiber. The simulated profiles are given by the equations below.

Constant "$\alpha = 1.835$"

$$X(r) = (13.5\%)\left(1 - \left(\frac{r}{25\ \mu\text{m}}\right)^{1.835}\right); \quad r < 25\ \mu\text{m} \tag{3}$$

"Core-Cladding Mismatch." This defect is qualitatively similar to that present in fiber 40 of the 108 fiber model used to quantify the installed fiber base of OM1 for the IEEE 802.3aq standard [26]

$$X(r) = (13.5\%)\left(1 - \left(\frac{r}{26\ \mu\text{m}}\right)^{1.835}\right); \quad r < 25\ \mu\text{m} \tag{4}$$

"α(r)"

$$X(r) = (13.5\%)\left(1 - \left(\frac{r}{25\ \mu\text{m}}\right)^{\alpha(r).}\right); \quad r < 25\ \mu\text{m} \tag{5}$$

where the radially dependent α has been fitted to the experimentally measured delays using 11 equally spaced points across the core which can take independent α values. The regions of the core between these points have α values which are linearly interpolated between these sample points. The resulting fit starts with $\alpha = 1.827$ at the centre of the core, mostly rises to a peak of 1.844 at 17.5 μm before falling to a level of 1.831 at 20 μm where it approximately stays until the cladding. For all simulated profiles the cladding is given by

$$X(r) = 0; \quad r >= 25\ \mu\text{m}. \tag{6}$$

E. Improving Modal Dispersion Over a 4.5 THz Optical Bandwidth With a Single Mask

Finally, the ability of a single phase mask to combat modal dispersion over a wide optical bandwidth is demonstrated. Fig. 9(a) contains the 3-dB roll-off frequency for each of the modes at 10 different wavelengths across the C-band. The modes share a single launch orientation which has been selected so as to optimize the worst-case wavelength. The general trend is consistent across the band; the first four mode-groups offer high bandwidth whilst there is increasingly poor performance for the higher-order modes. Although even the worst mode is still superior to the overfill launch condition. If a single strong modal-coupling event occurs somewhere along the fiber, say near the launch, it will cause a sharp null in the frequency response corresponding with the difference in propagation times of the two modes over the remaining distance. If coupling occurs in a more distributed fashion, there will still be a dip in the frequency response but it will be smoother, perhaps more akin to that visible in Fig. 6(a).

Due to the fact that the mode groups are approximately 140 ps apart there is a tendency for performance to have a dip near 7 GHz, with the depth of that dip depending on the degree of modal coupling. It is for this reason that so many of the modes have 3-dB roll-off points in the vicinity of 7 GHz. It should also be pointed out that although there is some genuine wavelength dependence to the frequency response, an example of which is shown in Fig. 9(b), when summarized in terms of 3-dB point as for Fig. 9(a) there is also noise in the measurements themselves. That is, even repeated measurements at the same wavelength give variations, particularly for mode-group 5 where mode-coupling is only just sufficient to cross the 3-dB threshold and remains flat near this threshold until approximately 15 GHz as can be seen in the purple series' of Fig. 7(a).

In addition to the frequency response measurements of Fig. 9 the suppression of modal dispersion was also demonstrated by taking eye diagrams for each of the wavelengths for the two best performing and lowest-order modes; $\text{LP}_{0,1}$ and $\text{LP}_{1,1}$ and this is illustrated in Fig. 10. Although $\text{LP}_{0,1}$ cannot be rotated, $\text{LP}_{1,1}$ was rotated so as to maximize the eye opening at 193.6 THz

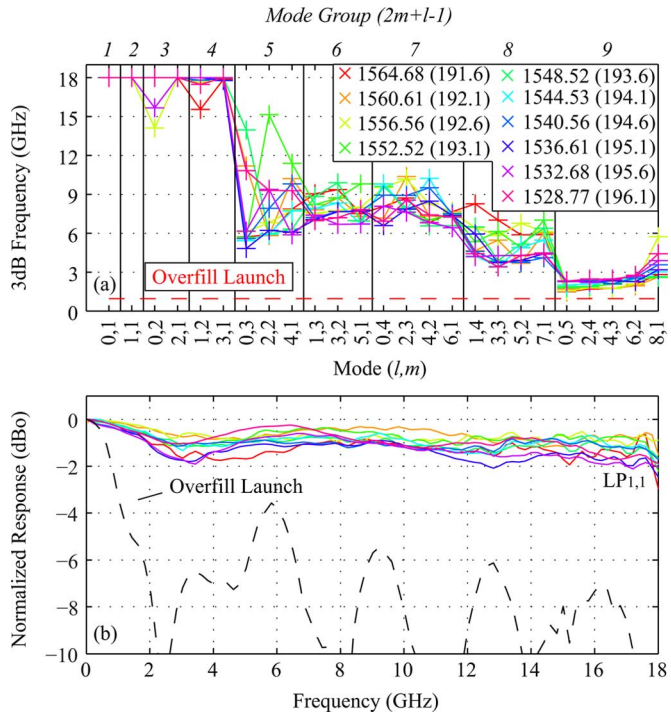

Fig. 9. (a) 3-dB roll-off frequency where each mode is orientated such that a single orientation maximizes the 3-dB point over the whole 4.5 THz bandwidth. (b) An example for the $\text{LP}_{1,1}$ mode at the same wavelengths as (a).

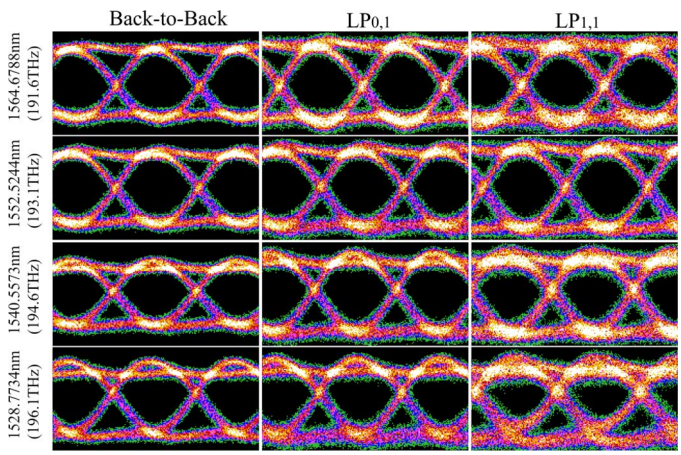

Fig. 10. 12.5 Gbps eye diagrams over 2 km at −12 dBm over a 4.5 THz bandwidth for the $\text{LP}_{0,1}$ and $\text{LP}_{1,1}$ modes, with a shared orientation for all wavelengths.

and the same orientation was used to take measurements for all wavelengths. It can be seen that the $\text{LP}_{0,1}$ mode is more stable over wavelength than the $\text{LP}_{1,1}$, although both modes manage to keep the eye open over the entire 4.5 THz band.

IV. Conclusion

This paper has demonstrated the use of binary phase masks with near perfect theoretical modal selectivity for the characterization of optical fibers and the suppression of modal dispersion in a single channel. More sophisticated phase masks will also become increasingly important in the context of MDM as the number of channels is increased and maintaining isolation between the modes becomes more difficult. By optimizing the

orientation of the modes, mode coupling was reduced, which is not only beneficial for telecommunications, but enables more accurate measurement of the modal characteristics of the fiber. Characteristics such as the propagation delay and chromatic dispersion of individual modes which in turn provide an estimate of the refractive index profile of the fiber.

ACKNOWLEDGMENT

The authors would like to thank the University of Cambridge Photonic Systems Group, and in particular, A. Wonfor for their assistance. The authors would also like to thank Hittite Microwave, Maxim IC, and Analog Devices for providing sample components.

REFERENCES

[1] D. H. Sim, Y. Takushima, and Y. C. Chung, "High-speed multimode fiber transmission by using mode-field matched center-launching technique," *IEEE J. Lightw. Technol.*, vol. 27, no. 8, pp. 1018–1026, Apr. 2009.

[2] R. Panicker, A. Lau, J. Wilde, and J. Kahn, "Experimental comparison of adaptive optics algorithms in 10-Gb/s multimode fiber systems," *IEEE J. Lightw. Technol.*, vol. 27, no. 24, pp. 5783–5789, Dec. 2009.

[3] L. Geng, S. H. Lee, K. A. William, R. V. Penty, I. H. White, and D. G. Cunningham, "Symmetrical 2-D Hermite Gaussian square launch for high bit rate transmission in multimode fiber links," in *Proc. Opt. Fiber Commun. Conf.*, 2011, paper OWJ5.

[4] G. Stepniak, L. Maksymiuk, and J. Siuzdak, "Binary-phase spatial light filters for mode-selective excitation of multimode fibers," *IEEE J. Lightw. Technol.*, vol. 29, no. 13, pp. 1980–1987, Jul. 2011.

[5] J. Carpenter and T. D. Wilkinson, "Holographic mode-group division multiplexing," in *Proc. Opt. Fiber Commun. Conf.*, 2011, paper OThN3.

[6] M. Salsi *et al.*, "Transmission at 2×100 Gb/s, over two modes of 40 km-long prototype few-mode fiber, using LCOS based mode multiplexer and demultiplexer," in *Proc. Opt. Fiber Commun. Conf. 2011*, paper PDPB9.

[7] C. Koebele *et al.*, "40 km transmission of five mode division multiplexed data streams at 100 Gb/s with low MIMO-DSP complexity," in *Proc. 37th Eur. Conf. Exposition on Opt.Commun.*, 2011, paper Th.13.C.3.

[8] R. Ryf, S. Randel, A. H. Gnauck, C. Bolle, R.-J. Essiambre, and P. J. Winzer, "Space-division multiplexing over 10 km of three-mode fiber using coherent 6×6 MIMO processing," in *Proc. Opt. Fiber Commun. Conf.*, 2011, paper PDPB10.

[9] E. Ip *et al.*, "$88 \times 3 \times 112$-Gb/s WDM transmission over 50 km of three-mode fiber with inline few-mode fiber amplifier," in *Proc. 37th Eur. Conf. Exposition Opt. Commun.*, 2011, paper Th.13.C.2.

[10] B. C. Thomsen, "MIMO enabled 40 Gb/s transmission using mode division multiplexing in multimode fiber," in *Proc. Opt. Fiber Commun. Conf.*, 2010, paper OThM6.

[11] S. Schöllmann, S. Soneff, and W. Rosenkranz, "10.7 Gb/s over 300 m GI-MMF using a 2×2 MIMO system based on mode group diversity multiplexing," in *Proc. Opt. Fiber Commun. Conf.*, 2007, paper OTuL2.

[12] A. Li, A. Al Amin, X. Chen, and W. Shieh, "Reception of mode and polarization multiplexed 107-Gb/s CO-OFDM signal over a two-mode fiber," in *Proc. Opt. Fiber Commun. Conf.*, 2011, paper PDPB8.

[13] H. S. Chen, H. P. A. Van den Boom, and A. M. J. Koonen, "30 Gbit/s 3×3 optical mode group division multiplexing system with mode-selective spatial filtering," in *Proc. Opt. Fiber Commun. Conf.*, 2011, paper OWB1.

[14] C. P. Tsekrekos and A. M. J. Koonen, "Mode-selective spatial filtering for increased robustness in a mode group diversity multiplexing link," *Opt. Lett.*, vol. 32, no. 9, pp. 1041–1043, May 2007.

[15] J. Xu and C. Peucheret, "Two-mode multiplexing at 2×10.7 Gbps over 7-cell hollow-core photonic band gap fiber," in *Proc. 37th Eur. Conf. Exposition Opt. Commun.*, 2011, paper We.10.P1.66.

[16] T. G. Euser *et al.*, "Dynamic control of higher-order modes in hollow-core photonic crystal fibers," *Opt. Exp.*, vol. 16, no. 22, pp. 17972–17981, Oct. 2008.

[17] S. Kirkpatrick, C. D. Gelatt, Jr., and M. P. Vecchi, "Optimization by simulated annealing," *Sci. New Series*, vol. 220, pp. 671–680, May 1983.

[18] A. W. Snyder and J. D. Love, *Optical Waveguide Theory*. London, U.K.: Chapman and Hall, 1983, p. viii, 734.

[19] J. H. Simmons and K. S. Potter, *Optical Materials*. London, U.K.: Academic Press, 2000, p. 104.

[20] T.-J. Ahn, Y. Jung, K. Oh, and D. Y. Kim, "Optical frequency-domain chromatic dispersion measurement method for higher-order modes in an optical fiber," *Opt. Exp.*, vol. 13, no. 25, pp. 10040–10048, Dec. 2005.

[21] D. Menashe, M. Tur, and Y. Danzinger, "Interferometric technique for measuring dispersion of higher order modes in optical fibers," *Electron. Lett.*, vol. 37, no. 24, pp. 1439–1440, Nov. 2001.

[22] J. W. Nicholson, S. Ramachandran, S. Ghalmi, E. A. Monberg, F. V. DiMarcello, M. F. Yan, P. Wisk, and J. W. Fleming, "Electrical spectrum measurements of dispersion in higher order mode fibers," *IEEE Photon. Technol. Lett.*, vol. 15, no. 16, pp. 831–833, Jun. 2003.

[23] Y. Jaouën, C. Palavicini, A.-F. Obaton, C. Moreau, and P. Sillard, "Direct chromatic dispersion determination of higher-order mode fibers using OLCR technique," in *Proc. Conf. Lasers Electro-Opt.*, 2005, Paper CThB4.

[24] G. D. Brown, "Chromatic dispersion measurements in graded-index multimode optical fibers," *IEEE J. Lightw. Technol.*, vol. 12, no. 11, pp. 1907–1909, Nov. 1994.

[25] C. D. Poole, J. M. Wiesenfeld, D. J. DiGiovanni, and A. M. Vengsarkar, "Optical fiber-based dispersion compensation using higher order modes near cutoff," *IEEE J. Lightw. Technol.*, vol. 12, no. 10, pp. 1746–1758, Oct. 1994.

[26] University of Cambridge OM1 BER Model Results Release 2.1 [Online]. Available: www.ieee802.org/3/aq/public/tools/108fiberModel/CamMMF2p1/

Author biographies not included at authors' request due to space constraints.